Polymer Degradation and Stability 99 (2014) 43–52

Contents lists available at ScienceDirect

Polymer Degradation and Stability

journal homepage: www.elsevier.com/locate/polydegstab

Synthesis of a novel dicyclic silicon-/phosphorus hybrid and its performance on flame retardancy of epoxy resin

Shiqiang Song, Jiajun Ma, Ke Cao, Guanjun Chang, Yawen Huang*, Junxiao Yang*

State Key Laboratory Cultivation Base for Nonmetal Composite and Functional Materials & School of Material Science and Engineering, Southwest University of Science and Technology, Mianyang 621010, People's Republic of China

ARTICLE INFO

Article history:
Received 8 March 2013
Received in revised form
28 October 2013
Accepted 7 December 2013
Available online 16 December 2013

Keywords:
Epoxy resin
Flame retardancy
Silicon-/phosphorus hybrid
Condensation polymerization

ABSTRACT

A novel silicon-/phosphorus hybrid (SDPS) was synthesized by a condensation polymerization of diphenylhydroxysilane and spirocyclic pentaerythritol di(phosphate monochloride). The use of SDPS and the cooperative use of SDPS with P–N hybrid in flame retardant epoxy resin (EP) were investigated. Limiting oxygen index and cone calorimeter tests showed that the loading of SDPS and the cooperative use of SDPS and P–N hybrid in EP provided enhanced fire resistance. TGA, TG-FTIR and SEM measurements revealed that the enhancement in fire resistance was arising from the formation of a compact honeycomb carbonaceous structure hybridized by silica, the good char forming ability and the inhibition of flammable gas release. Further analysis from Raman spectra revealed that the compact carbonaceous layer may be originated from an increase in ordering of amorphous carbonaceous layer.

© 2013 Elsevier Ltd. All rights reserved.

1. Introduction

Epoxy resins are globally used on a large scale for microelectronics packaging materials, biotechnology, mechanical engineering and environment engineering, owing to their excellent moisture, solvent and chemical resistances, low shrinkage on cure, toughness, high adhesion to many substrates and superior electrical resistance property [1,2]. Flame-retardant treatment of epoxy resins by introducing halogens (mainly Cl and Br) was most widely used. However, the uses of halogen-containing additives are evoking the environment issue as they produce toxic gases such as dioxine and furane, during their combustion [3]. Recently, some ecological and friendly flame retardants have been developed to improving burning resistance of epoxy resins, involving natural mineral (montmorillonite, kaolinite, aluminum hydroxide et al.) [4,5], phosphorous-, nitrogen-, boracium- and silicon-containing compounds [6–8].

Phosphorus-containing compounds have shown promising application as halogen-free, flame retardants in epoxy resins [9–11]. On one hand, phosphorus-containing compounds can hindrance combusting of H or OH·, thus reducing the energy of flame in the gas phase. On the other hand, they generally convert into polyphosphoric acid in the solid phase during decomposition, consequently catalyzing the formation of a protective carbonaceous layer, which is highly thermal stability and can retard further decomposition of polymer chains. Moreover, research about the flame retardancy of epoxy resins has shown a high independency on the phosphorus contents. Increase of phosphorus contents can effectively improve the flame retardancy of resins. However, high loading of additive-type phosphorus-containing compounds destroyed the mechanical properties and the thermal stability and led to outflow phenomenon, further lowering the efficiency of the flame retardant. Thus, phosphorus/nitrogen combined systems have been developed. Most of these systems are based on phosphorus-/nitrogen-containing compounds, such as ammonium polyphosphate (APP), and melamine phosphate (MP). In addition, these compounds were commonly used in assistance with polyatomic alcohol like pentaerythritol (PER), consequently constructing intumescent flame retardation (IFR) composed by a blowing agent, a carbonization agent, and an acid source.

Silicon-containing compounds have also aroused much attention [12,13]. Compared with phosphorus/nitrogen containing compounds, silicon-containing compounds are regarded as an environmentally friendly flame retardant. More importantly, they could migrate to the surface of polymer matrix at high temperature due to their low surface energy, forming a protective silica layer to hamper the penetration of air and heat into polymers. However, some studies have shown that silicone-containing compounds [14,15], e.g., polydimethylsiloxanes (PDMS), show unsatisfied flame retardancy.

* Corresponding authors. Tel./fax: +86 816 2419076.
E-mail addresses: huangyawen@swust.edu.cn (Y. Huang), yangjunxiao@swust.edu.cn (J. Yang).

0141-3910/$ – see front matter © 2013 Elsevier Ltd. All rights reserved.
http://dx.doi.org/10.1016/j.polymdegradstab.2013.12.013

In recent years, the P and Si combined system have been intensively investigated and presented highly improved flame retardancy [16–26]. For example, Schartel et al. reported a P and Si combined flame retardant by cooperatively using Si-based and P-based FR. The fire retardancy in PC composites was caused by both flame inhibition in the gas phase and inorganic-cabonaceous residue formation in the condensed phase [16–20]. Chen et al. reported a new flame retardant containing silicon and caged bicyclic phosphate for polyamide 6. The condensed phase action was considered as the major flame retardancy mechanism with the fuel reduction action as the minor [21]. In the study of Sponton et al., silicon-based and phosphorus-based compounds were directly incorporated into the chemical structure of polybenzoxazines to enhance the flame retardancy. The fire retardancy mechanism was described as that silicon provides an enhancement of the thermal stability of the char [22]. Yang et al. synthesized a novel P/Si hybrid FR (DOPO-POSS). Its use in epoxy resin, polyamide and polycarbonate were investigated, respectively. An interesting blowing-out effect or synergistic effect of P/Si were reported [23–25]. Overall, most current P and Si combined systems generally involved the blends of P-based and Si-based FRs or small molecular P/Si hybridized system. Polymeric P/Si hybridized systems, whose P-based and Si-based moieties were linked by chemical bonds, were seldom reported. Compared with conventional P/Si-combined systems, P/Si hybridized polymeric structures would show some special flame retardant properties. First, polymeric structures enabled chain entangling and chain folding, consequently leading to high local concentration of phosphorus-related acidic catalysts and possibly facilitating the char formation. Second, the P-based units were linked with Si-based units by relatively weak P–O–Si bonds, whose scission simultaneously produced active P and Si-containing moieties. As a consequence, the phosphorous catalyzed char forming and the silica forming processes may tend to take place synchronously. This may be helpful to enhance the barrier effect of charring layers.

In this work, a novel silicon-/phosphorus-containing flame retardant (SDPS) was synthesized by condensation polymerization of diphenylhydroxysilane and spirocyclic pentaerythritol di(phosphate monochloride) (SPDPC). This new flame retardant is characteristic of polymeric structure with P–O–Si linkages in mainchains. To construct an intumescent system, SDPS was cooperatively used with mono (4, 6-diamino-1,3,5-triazin-2-aminium) mono (2,4,8,10-tetraoxa-3,9-di-phosphaspiro [5.5] undecane-3, 9-bis (olate) 3, 9-dioxide) (SPDM), which was a well-established P–N intumescent flame retardant. The flame retardancy performance of epoxy resin/SDPS and epoxy resin/SDPS/SPDM composites were evaluated by LOI and cone calorimeter tests. Thermal decomposition property, char residue structure and morphology, gas evolution of epoxy resin composites has been characterized by TGA, FTIR/EDS, SEM, Raman and TG-FTIR, respectively. Finally, the flame retarding mechanism was investigated.

2. Experimental

2.1. Materials

Phosphorus oxychloride ($POCl_3$), Pentaerythritol (PER), tripolycyanamide (MA), triethanolamine (TEOA) and other common solvents (Chengdu Kelong Reagent Co.) were purified with standard methods before used unless noted otherwise. Diphenyldichlorosilane (China Bluestar Chengrand Chemical Co.), Methyl hexahydrophthalic anhydride (MHHPA, Puyang Huicheng Chemical Co.), Epoxy resin, diglycidyl ether of biphenol A, DEGBA, with epoxy value of 0.4083 mol/100 g (Lanzhou Bluestar Resin Co.) were used without further purification. Diphenylsilanediol (DPSD) was synthesized via the method reported by Burkhard [18].

2.2. Synthesis of 3, 9-dichloro-2, 4, 8, 10-tetraoxa-3, 9-diphosphaspiro [5. 5] undecane 3, 9-dioxide (SPDPC) [19]

In a 1000 mL glass flask equipped with a magnetic stirrer, a thermometer, a circumference condenser and heating bath, pentaerythritol (PER) (1.0 mol) and phosphorus oxychloride ($POCl_3$) (11.0 mol) were mixed at room temperature. Then, the temperature was elevated slowly to 105–110 °C. The reaction was conducted for more than 20 h until HCl was not eluted. The raw product was filtered and washed by dichloromethane (CH_2Cl_2), tetrachloromethane (CCl_4) and ether sequentially. The product was dried to constant weight at 50 °C in vacuum oven, producing a white solid powder (yield: 82%).

2.3. 3-((Methoxydiphenylsilyl) oxy)-9-methyl-2, 4, 8, 10-tetraoxa-3, 9-diphosphaspiro [5. 5] undecane 3, 9-dioxide (SDPS)

SPDPC (29.7 g, 0.1 mol) were added in a 250 mL glass flask and dispersed by acetonitrile (100 mL) at room temperature, and then the temperature was elevated to 80 °C slowly. When SPDPC was fully dissolved, diphenylsilanediol (DPSD) (20.7 g, 0.15 mol) was added to the solution at once. The reaction was conducted at 80–85 °C for 18 h under stirring and N_2 environment. The solution was charged into ethanol, producing a white solid power. The white solid powder was washed with ethanol and ether sequentially, and then dried to constant weight at 50 °C in vacuum oven.

2.4. Mono (4, 6-diamino-1, 3, 5-triazin-2-aminium) (2, 4, 8, 10-tetraoxa-3, 9-diphosphaspiro [5. 5] undecane-3, 9-bis (olate) 3, 9-dioxide) (SPDM) [27]

In a 250 mL glass flask, SPDPC (14.9 g, 0.05 mol), tripolycyanamide (12.6 g, 0.1 mol) and deionized water (125 mL) were mixed at room temperature in N_2 environment. Then the temperature was elevated to 100 °C slowly and kept for more than 15 min. Resultant solution was allowed for cooling at room temperature to produce precipitates. The precipitates were washed with cold water for several times and then dried to constant weight at 50 °C in vacuum oven, producing a white solid power. FTIR data: 3412 cm^{-1} (NH_2), 1618 and 1515 cm^{-1} (C=N), 1255 cm^{-1} (P=O) and 1025 cm^{-1} (P–O); ^1H NMR data: 7.4 ppm (PO_3–H^+), 3.9 ppm (NH_2), 3.4 ppm (CH_2); ^{13}C NMR data: 160.1 ppm (C=N), 67.8 ppm (PO–C), 35.4 ppm (C*-C4).

2.5. Preparation of epoxy composites

Epoxy resin (EP) and flame retardants (5.5 wt. % or 10.4 wt. % of epoxy resin) were added into a three-necked flask equipped with a mechanical stirrer. The mixture was heated at 90 °C until flame retardant was completely disperse in EP to form homogeneous system. Then curing agent, methyl hexahydrophthalic anhydride (MHHPA, 68.8 wt. % of EP) and accelerating agent, triethanolamine (TEOA, 2.0 wt. % of EP), were added sequentially. The reaction mixtures were pre-cured in a mould at 100 °C for 1 h, followed by a final curing at 120 °C for another 2 h, giving rise to pellet solid resins.

2.6. Characterization

Fourier transform infrared (FTIR) spectra were obtained on a Perkin Elmer Spectrum One spectrophotometer with a resolution of 2 cm^{-1}. Raman spectroscopy was recorded on Via-Reflex confocal laser Raman spectrometer (Renishaw Ltd) with a resolution of 2 cm^{-1}. ^1H and ^{13}C NMR spectra were collected on a Bruker Acance spectrometer (400 MHz) using tetramethylsilane (TMS) as internal reference and deuterated dimethyl sulfoxide (DMSO-d_6) as solvent.

Thermogravimetric analysis (TGA) was performed on a TA SDT Q600 at a heating rate of 20 °C/min under air. Limiting oxygen index (LOI) was determined on a LFY-606 oxygen index instrument (Qingdao, China.) with a test specimen bar of 100 mm × 6 mm × 4 mm according to ASTM D-2863. Flammability of epoxy resin and their composites was also characterized using a cone calorimeter performed in Stanton Redcroft, UK device according to ISO 5660 with an incident flux of 35 kW m^{-2} using a cone shape heater. Scanning electron microscopy of fracture surface of composites was recorded on a TM-1000 (Hitachi Ltd) scanning electron microscope at an accelerating voltage of 10 kV. Dynamical mechanical analysis (DMA) was performed on a TA Q800 dynamical mechanical analyzer in three-point bending mode at a frequency of 1 Hz. TG-IR instrument consists of analyzer (TGA-Q5000, TA Company, USA) coupled with Fourier transform spectrometer (Nicolet 6700) via a transfer line. TG was carried out at a heating rate of 20 °C/min and a flow rate of 80 mL/min under air atmosphere.

3. Results and discussion

3.1. Preparation of the flame retardants

Synthesis routes to SDPS and SPDM are shown in Scheme 1. SDPS was synthesized via a condensation polymerization of SPDPC and diphenylhydroxysilane in the presence of triethoxyamine. The products can be precipitated from acetonitrile to ethanol, which is an obvious evidence of an occurrence of high molecular weight compounds. FTIR spectra of SDPS, DPSD and SPDPC are depicted in Fig. 1. In the spectrum of SPDS, one can find that the characteristic absorption peak of −OH groups at 3237 cm^{-1} and P−Cl at 546 cm^{-1} disappeared and that of P−O−Si at 1080 cm^{-1} appeared [28]. This demonstrated a condensation reaction between P−Cl of SPDPC and −OH of diphenylhydroxysilane. Moreover, the absorption bands at 1280 and 1200 cm^{-1} assignable to the P═O and P−O−C bonds appeared [29,30]. The structure of SDPS was further confirmed by ^{1}H and ^{13}C NMR (Fig. 2). ^{1}H NMR spectrum (Fig. 2a) presents two main proton signals at 4.0–4.5 and 7.0–7.8 ppm, which correspond to the $-CH_2$ protons of spiro structure and the Ar−H protons, respectively. The existence of two peaks of $-CH_2$ protons could be attributed to the stable chair conformation of hexatomic rings, resulting in a unequivalence of hydrogen atoms locating at axial and equatorial bonds. This further revealed that the spiro structure of SPDPC was well preserved in the condensation reaction of P−Cl bond with Si-OH. The peaks at δ = 35.7–35.9 ppm in ^{13}C NMR

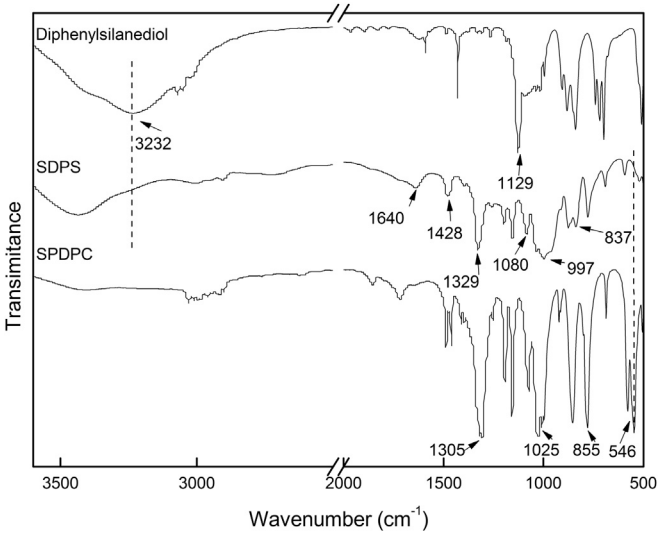

Fig. 1. FTIR spectra of SPDPC, diphenylhydroxysilane and SDPS.

spectrum (Fig. 2b) could be assigned to quaternary carbon atom in the spiro moiety. The peaks at 68.1–68.3 and 125–135 ppm were assignable to the carbons at $-C^{*}H_2-O-P$ and benzene carbons, respectively.

Molecular weight of SDPS is attainable by ^{1}H NMR integration. The integration result shows that the ratio of signal intensity of phenyl hydrogen to that of methylene hydrogen is 1:0.91. Hence, the DPSD/SPDPC ratio in SDPS can be calculated according to the hydrogen number of SPDPC and DPSD. The calculated ratio is 0.1:0.114, indicating that the terminal groups of polymers are SPDPC. This is linked with the excessive feed amount SPDPC relative to that of DPSD. The degree of polymerization, n, can be simply obtained by following equation:

$$\frac{n+1}{n} = 0.114/0.1$$

so n is approximately 7. The molecular weight can be calculated by: $(M_{SPDPC} + M_{DPSD} - M_{HCl}) \times 7 + M_{SPDPC} - M_{Cl} + M_{OH}$

The obtained value is 3486 g/mol. Further, the calculated phosphorus content of SDPS is 14.4 wt%.

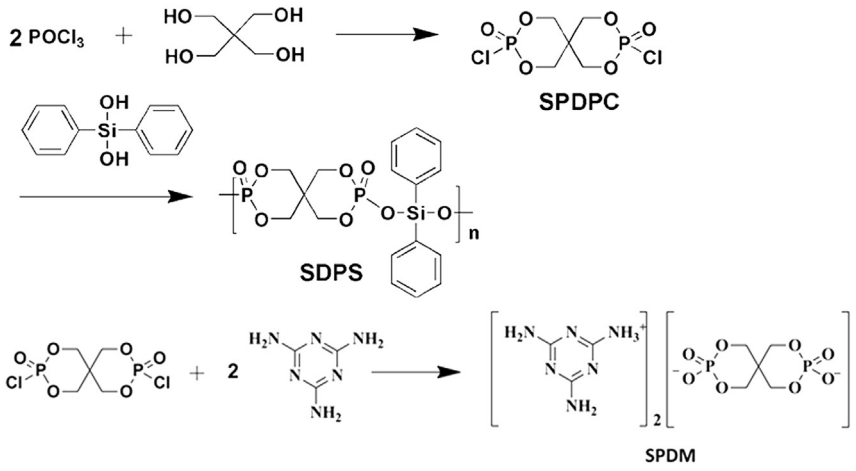

Scheme 1. Synthetic routes to SDPS and SPDM.

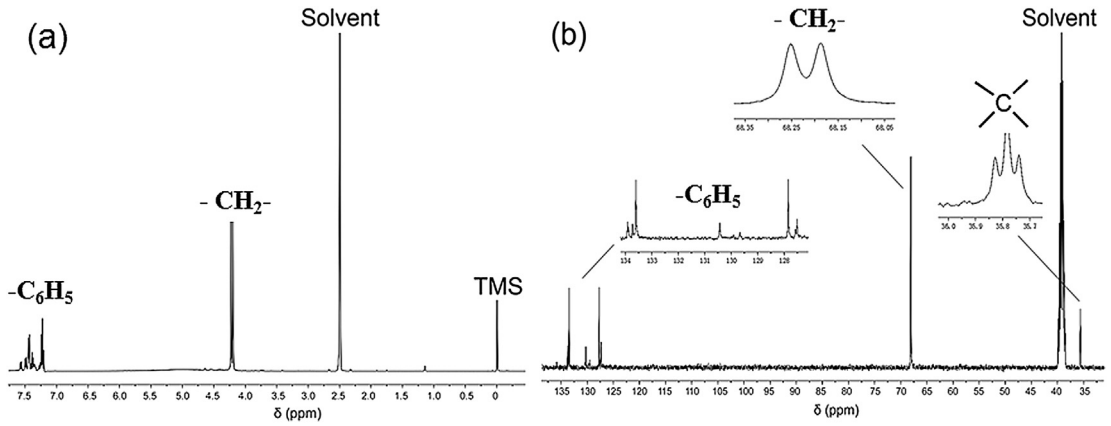

Fig. 2. ^{1}H NMR (a) and ^{13}C NMR (b) spectra of SDPS.

3.2. Thermal degradation of SDPS

Understanding thermal degradation properties of flame retardants is helpful to reveal its flame retarding mechanism. In this work, TGA/DTG, SEM-EDS, TG-IR and FTIR were employed to investigate the decomposition behavior of SDPS. As shown in TG curve of SDPS (Fig. 3a), the decomposition of SDPS shows a major weight loss at the range of 300–500 °C. DTG curves of SDPS further depict three-step decomposition in air with corresponding T_{max} (temperatures of maximum weight loss rate) of 358, 485 and 745 °C, respectively (the weight loss at 100–200 °C is attributed to the release of water). The char residual weight ratio at 600 °C and 800 °C were approximately 40 wt.% and 20 wt.%, respectively. SEM image of the char residue at 400 °C shows a loose carbonaceous morphology (Fig. 3a). EDS measurement results (Fig. 3b) indicate that the char residues consist of a large amount of P and Si elements, implying that P and Si mainly exist in solid phase as polyphosphates and silica without considerable evolution into gas phase.

Chemical structure of condensed phase and released gas compounds during the thermal degradation of SDPS in air was further investigated by FTIR and TG-IR, respectively. Fig. 4 depicts the FTIR spectra of SDPS heated at 100, 200 and 400 °C. Comparing the spectra of different temperatures, one can find that the spectrum at 400 °C is obviously different with other spectra, indicating a significant chemical structure change. In detail, the absorption bands of P═O stretching at nearly 1280 cm^{-1}, P–O–C stretching at 1200 cm^{-1} and P–O–Si stretching at 1080 cm^{-1} greatly decreased. In the meantime, broad adsorption bands appear at 1170, 1000 and 492 cm^{-1},indicating the appearance of new compounds such as polyphosphoric acids and silica [31]. Fig. 5 shows FTIR spectra of the evolved gas of SDPS at the main decomposition temperatures of SDPS. The evolved gas analysis exhibit characteristic bands of aromatics (3080 cm^{-1}), hydrocarbons (2942 cm^{-1}), CO_2 (2360 cm^{-1}) and P–O compounds (1100 cm^{-1}), respectively [21,30]. The existence of hydrocarbons at about 300 °C indicates the break of P–O–C bond and degradation of char residue. The peak of P–O compounds should be arising from the break of P–O–Si bonds.

3.3. Preparation and flammability of epoxy composites

SDPS, SPDM and SDPS/SPDM were incorporated into epoxy resin to prepare composites. The compositions and limiting oxygen index (LOI) of the composites were listed in Table 1. The flame retardants contents used in this work were 5.5, 10.4 and 15 wt%, respectively. As a typical P–N hybrid flame retardant, SPDM was used for comparison and was also jointly used with SDPS. LOI measurement results show that both EP/SDPS and EP/SPDM composites exhibit higher LOI value than pristine EP. When increasing loading content of SDPS and SPDM from 5.5 to 10.4 wt.%, the LOI values were further elevated. However, when increasing the content of SDPS from 10.4 wt.% to 15 wt.%, the LOI values only showed a slight increase. Moreover, LOI values of EP/SDPS composites were higher than that of EP/SPDM composites, in particular, EP/SDPS-2

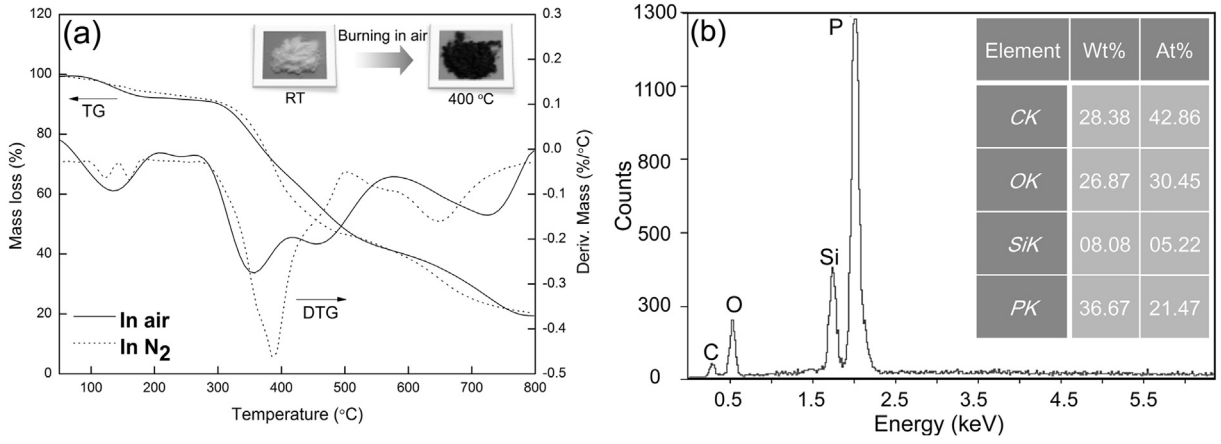

Fig. 3. Thermal property of SDPS: a) TGA and DTG curve of SDPS under air (solid line) and N_2 (dotted line); b) EDS spectrum of char residual at 400 °C.

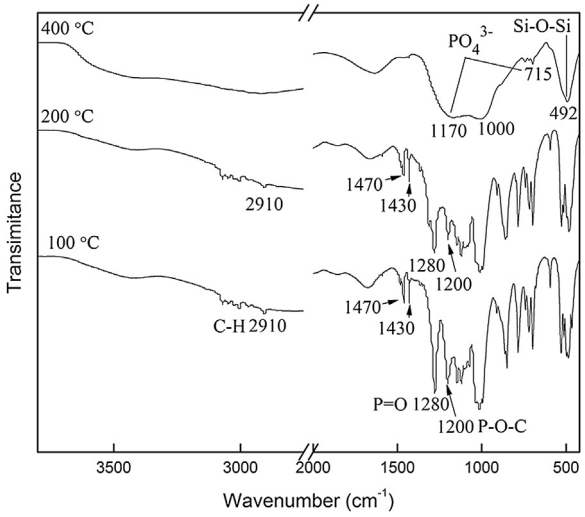

Fig. 4. FTIR spectra of SPDS under heating at 100, 200 and 400 °C, respectively.

exhibited a high LOI value of 28.9%. These results demonstrate the possible appearance of P–Si synergistic effect which leads to a superior flame retarding performance over SPDM. The cooperative use of SDPS and SPDM with the ratio of 1:1 in EP led to a further increase of LOI value to 30.8% and 32.1%, when the FR contents were 10 and 15 wt.%, respectively. These values were apparently higher than the LOI values attained from using SDPS and SPDM alone. However, the use of SDPS/SPDM ratios of 3:1 and 1:3 showed considerably low LOI values of 27.5 and 26.5%. Thus, it can be concluded that LOI values of EP/SDPS/SPDM composites greatly depended on SDPS/SPDM ratios and the enhancement in fire retardancy can take place only when the flame retarding effect of SDPS and SPDM was well balanced. Revealing how to achieve such type of balance is crucial to understand the flame retarding mechanism.

Fig. 6 shows the combustibility curves of neat EP, EP/SDPS-2 and EP/SDPS/SPDM-2. Related data including heat release rate (PHRR), the total heat release (THR), the average mass loss rate (AMLR), and smoke generation rate are summarized in Table 2. As can be seen, the loading of SDPS in EP resulted in an obvious reduction in PHRR, demonstrating good fire retardancy of EP/SDPS. In contrast to EP/SDPS, EP/SDPS/SPDM composite shows higher reduction

Table 1
The compositions and LOI values of Neat EP, EP/SDPS, EP/SDPM and EP/SDPS/SPDM composites.

Samples	DEGBA/g	MHHPA/g	TEOA/g	SDPS/g	SPDM/g	FRs/ wt%	LOI (%)
Neat EP	52.3	36.6	1.05	0	0	0	20.2
EP/SDPS-1	49.6	35.2	1.0	4.96	0	5.5	24.1
EP/SDPS-2	47.0	33.3	0.94	9.41	0	10.4	28.9
EP/SDPS-3	44.8	30.8	0.90	13.5	0	15%	29.4
EP/SPDM-1	49.6	35.2	1.0	0	4.96	5.5	23.2
EP/SPDM-2	47.0	33.3	0.94	0	9.41	10.4	25.1
EP/SPDM-3	44.8	30.8	0.90	0	13.5	15%	27.2
EP/SDPS/SPDM-1	47.0	33.3	0.94	7.06	2.35	10.4	27.5
EP/SDPS/SPDM-2	47.0	33.3	0.94	4.71	4.71	10.4	30.8
EP/SDPS/SPDM-3	47.0	33.3	0.94	2.35	7.06	10.4	26.5
EP/SDPS/SPDM-4	44.8	30.8	0.90	10.13	3.37	15%	28.8
EP/SDPS/SPDM-5	44.8	30.8	0.90	6.75	6.75	15%	32.1
EP/SDPS/SPDM-6	44.8	30.8	0.90	3.37	10.13	15%	27.6

(approximately 35.3%) in PHRR to some degree. This result was consistent with LOI test result.

3.4. Morphology of fracture surfaces of EP and EP composites

Scanning electron micrography (SEM) was used to determine the microscopic fracture surface morphology of neat EP, EP/SDPS, EP/SPDM and EP/SDPS/SPDM composites. SEM image of EP shows a smooth fracture surface (Fig. 7a), reflecting a homogeneous structure. Similar morphology without phase separation was also observed in the SEM image of EP/SDPS (Fig. 7b), indicating a good dispersion of SDPS but a poor interfacial interaction between EP and SDPS. In comparison, EP/SPDM and EP/SDPS/SPDM show a number of micro-sized particles and a rough fracture surface with a platelet-like morphology (Fig. 7c–d). The micro-sized particles should be attributed to the aggregation of SPDM molecules, suggesting a poor dispersion of SPDM. However, the rough fracture surface apparently evidences that a toughening mechanism was dominant in the EP composites, thus supporting a strong interfacial interaction [32].

3.5. Dynamic mechanical analysis, DMA

Dynamic mechanical analysis (DMA) is an effective tool for the characterization of the interfacial interaction of filled polymer systems, especially the damping spectra. Fig. 8 shows the storage

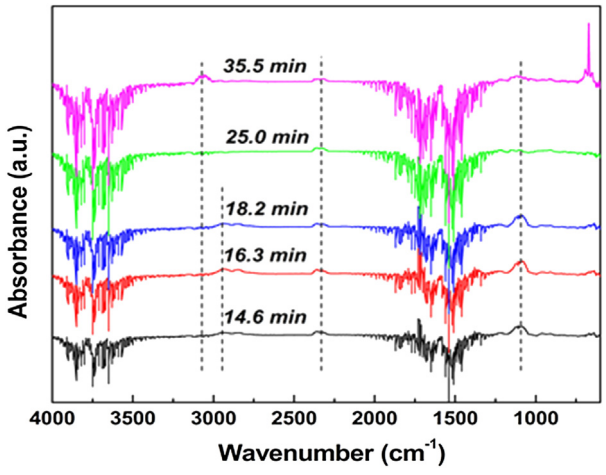

Fig. 5. FTIR spectra of the evolved gas of SDPS at 14.6, 16.3, 18.2, 25.0 and 35.5 min.

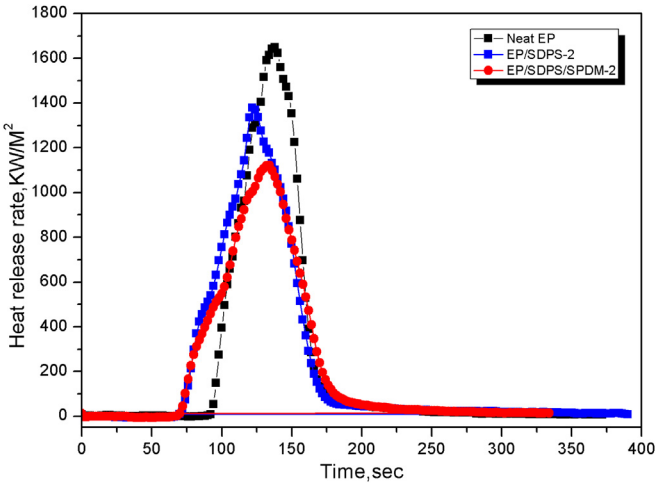

Fig. 6. Heat release rate curve for neat epoxy resin, EP/SDPS-2 and EP/SDPS/SPDM-2.

Table 2
Cone calorimeter data for neat epoxy resin and composites with a loading of 10 wt% of SDPS and SDPS/SPDM.

Formulation	t_{ign} s	t_{PHRR} s	PHRR kW m^{-2}	THR MJ m^{-2}	AMLR g s^{-1}
Neat EP	86	138	1650	213	0.0837
EP/SDPS-2	62	122	1378	203	0.0828
EP/SDPS/SPDM-2	62	134	1122	207	0.0706

modulus and Tan (δ) of neat epoxy resin, EP/SDPS, EP/SPDM, and EP/SDPS/SPDM composites with filler loading of 10.4 wt% as a function of temperature. The glass transition temperatures (T_g) of neat EP and EP composites were extracted in terms of the peak temperature of Tan (δ)–T curves. T_g of the polymer composites is determined by the dispersion of flame retardants and the interfacial interaction. EP/SPDM presents higher T_g while EP/SDPS presents a close T_g in contrast to EP. The storage modulus of EP/SDPS at glassy state is also greatly lower than that of EP/SPDM. Further consideration is given by the T_g dispersion depicted in Fig. 8. The internal friction peak width described by T_s/T_g (T_s is the temperature of maximum decrease rate in the storage modulus) was used, which has been found to be correlated to the interfacial structure between flame retardants and EP matrixes. The increase in T_s/T_g generally implies an enhancement in the homogeneity [33]. The order of T_s/T_g is EP/SDPS > EP/SDPS/SPDM > EP/SPDM. This suggests a better homogeneity of EP/SDPS and a better heterogeneity of EP/SPDM. In terms of above analysis, it can be concluded that EP/SPDM has a strong interfacial interaction while EP/SDPS has a relatively weak interfacial interaction. This conclusion was in agreement with that obtained from SEM (Fig. 7). Moreover, EP/SDPS/SPDM exhibited higher T_g of 94 °C than that of EP/SDPS and EP/SPDM. This is, we believe, because that the cooperative

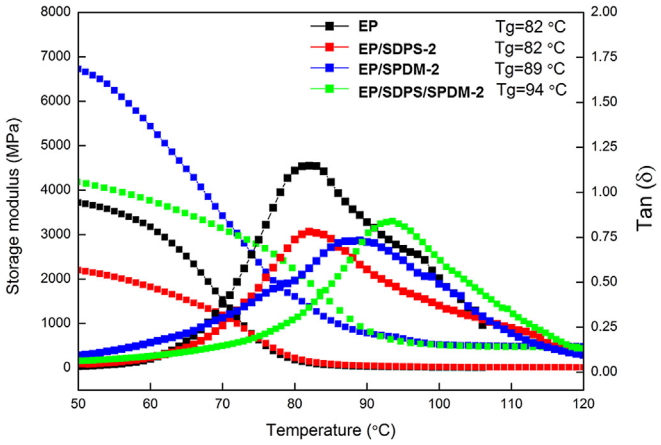

Fig. 8. DMA curves of neat EP, EP/SDPS-2, EP/SPDM-2 and EP/SDPS/SPDM-2.

incorporation of SDPS and SPDM leads to a combination of good dispersion and strong interfacial interaction. This may be responsible for the highly enhanced flame retarding performance of EP/SDPS/SPDM.

3.6. Thermogravimetric analysis of EP and EP composites

Thermal properties of EP composites were investigated by TGA. Fig. 9 shows the TGA curves of EP and EP composites and Table 3 summarizes the TGA data. The loading of SDPS, SPDM and their mixtures into EP led to a facilitated decomposition of EP in the range of 300–400 °C and an increase in residue weight ratio at 600 °C from 5.9 wt% to above 10 wt% (Fig. 9a–b). Both the

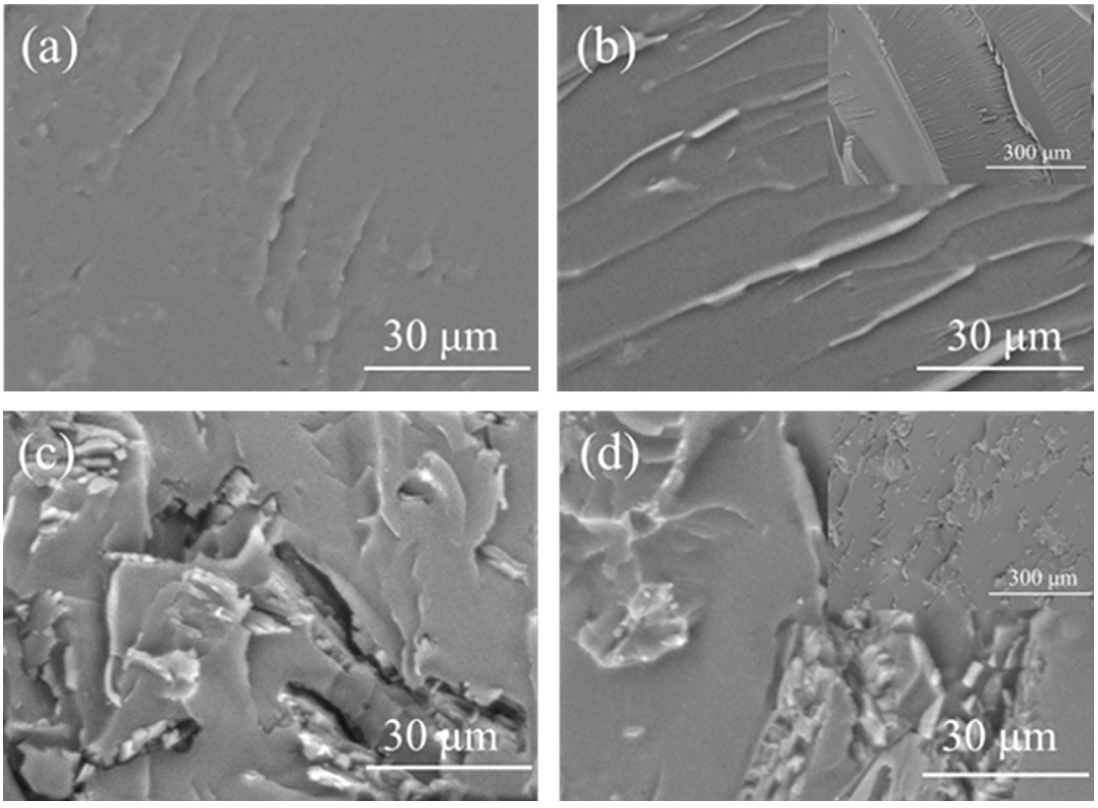

Fig. 7. SEM images of fracture surface: NEP (a), SDEP-2 (b), SPEP-2 (c) and SD/SPEP-2 (d).

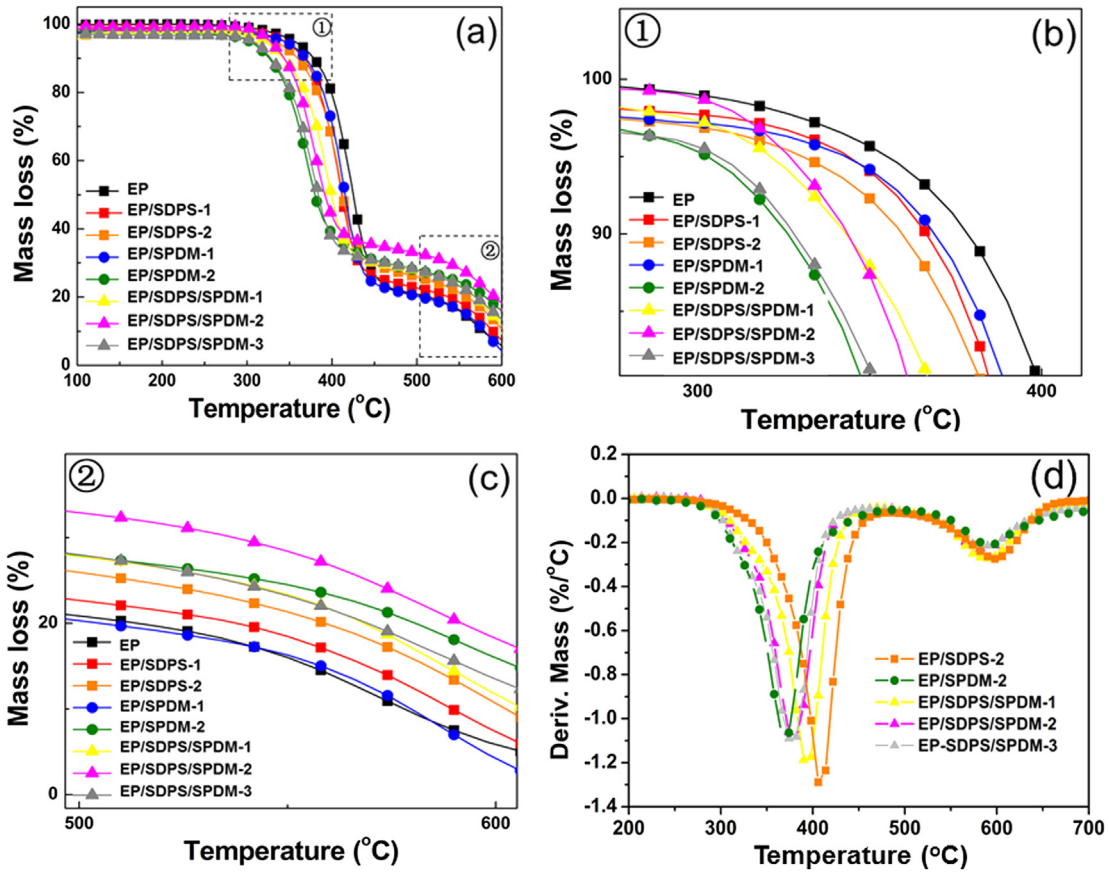

Fig. 9. TGA curves of the cured resins (a) and enlarged view of TGA curve around the initial decomposition temperature (b), enlarged view of TGA curve at 500–600 °C (c). ΔM (*T*) curve of the composites with different amounts of SDPS and SPDM (d).

facilitated decomposition and the increase in residue weight ratio were related to the catalyzed char forming process. Fig. 9c–d depict the TGA curves at the range of 300–400 °C and DTG curves. The comparison among TGA and DTG results of EP/SDPS, EP/SPDM and EP/SDPS/SPDM composites provides following information: 1) EP/SPDM composite showed lower decomposition temperature ($T_{5\%}$ = 305 °C) and higher residue weight ratio (15.9 wt.% at 600 °C) than EP/SDPS composite ($T_{5\%}$ = 330 °C; 10.7 wt.% at 600 °C) (Table 3). We suggest that the relatively low decomposition temperature of EP/SPDM may be related to the relatively poor thermal stability of SPDM (Fig. S1), consequently releasing phosphates at lower temperature and resulting in more pronounced facilitation of EP degradation. However, such a facilitated decomposition and enhanced char forming ability didn't result in a good fire resistance of EP/SPDM composite (Table 1). This result reveals that the flame retarding performance of EP/SDPS is not determined by the char forming ability alone, but is also related to other factors, such as the compactness of charring layer. 2) SDPS/SPDM ratio shows a significant effect on thermal properties of corresponding EP/SDPS/SPDM composites. In particular, the use of SDPS/SPDM ratio of 1:1 in EP led to a considerable larger residue weight ratio of 18.3 wt% than other EP-SDPS/SPDM composites, which reflects an outstanding char forming ability. This may contribute to the best flame retarding performance of EP/SDPS/SPDM-2. 3) $T_{5\%}$ of EP-SDPS/SPDM-1, EP-SDPS/SPDM-2 and EP-SDPS/SPDM-3 are 327, 321 and 303 °C, respectively, all of which are between that of EP/SPDM and EP-SDPS composites. DTG curves show that T_{max} of EP-SDPS/SPDM is also between that of EP-SPDM and EP-SDPS. It is reasonable to conclude that the catalysis by SDPS and SPDM on the degradation processes of EP induced an enhancement in char forming without altering degradation mechanism. Moreover, the facilitation in char forming was also supported by AMLR and THR analysis result (Fig. 9a) [34]. Overall, TGA results reveal that the enhancement of fire retardancy for EP/SDPS/SPDM should be attributed to a high charring residual weight ratio. However, such high weight ratio is not simply originated from the catalyzed char forming process.

Table 3
TGA data of neat EP and EP composites.

Samples	$T_{5\%}$ (°C)	T_{10}% (°C)	T^1_{max} (°C)	T^2_{max} (°C)	Residue weight ratio at 600 °C (%)
Neat EP	355	378	422	574	5.9
EP/SDPS-2	330	359	406	582	10.7
EP/SPDM-2	303	326	406	598	15.9
EP/SDPS/SPDM-1	321	343	390	590	11.8
EP/SDPS/SPDM-2	327	344	382	582	18.3
EP/SDPS/SPDM-3	306	328	374	590	13.5

3.7. Char morphology and architecture

The morphology and architecture of char residue recorded by SEM is shown in Fig. 10. SEM image of char residue of neat EP resin clearly shows a seriously damaged morphology without forming protective layer (Fig. 10a). This should be responsible for the poor fire resistance of EP. In comparison, char residue of EP/SDPS and EP/SPDM composites showed relatively compact but open porous architecture (Fig. 10b–c). Such open porous architecture presents

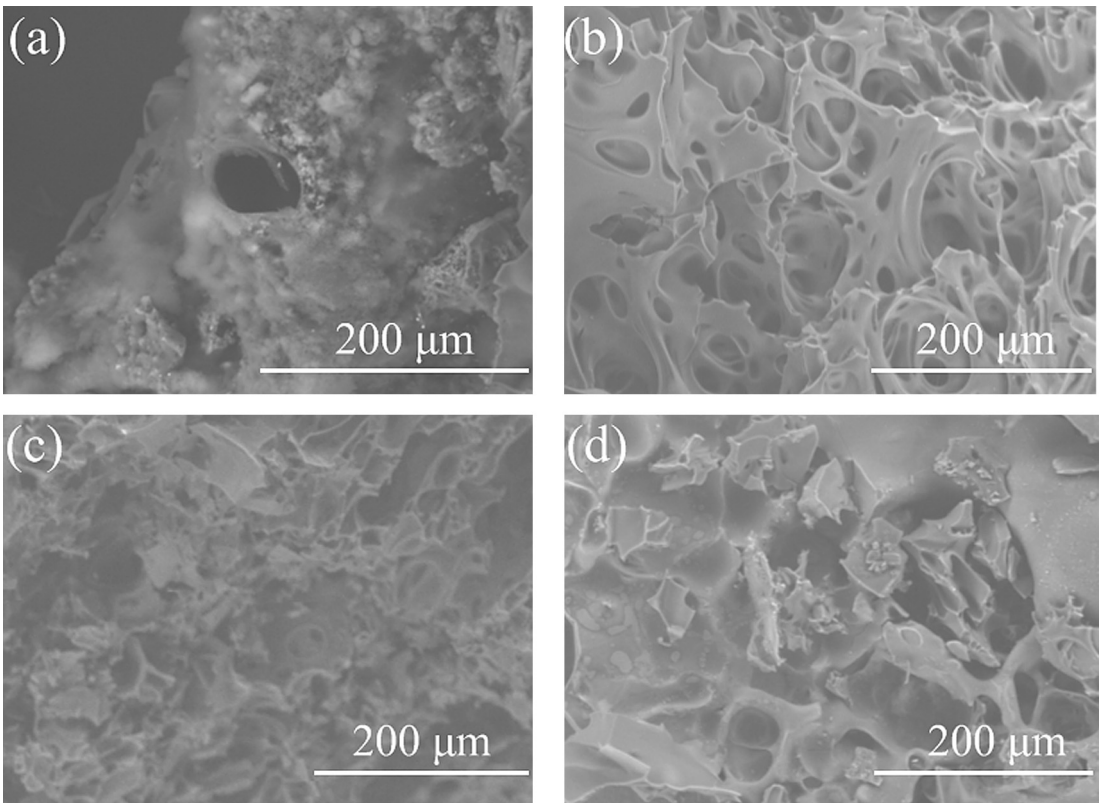

Fig. 10. SEM images and Raman spectra of char residual: Neat EP (a), EP/SDPS-2 (b), EP/SPDM-2 (c) and EP/SDPS/SPDM-2 (d).

disadvantage in isolating the gas and heat. In these two composites, EP/SDPS appeared to display smaller-sized porous and more compact surface architecture. This explains that EP/SDPS exhibited better fire resistance although it has lower residue weight ratio in contrast to EP/SPDM as mentioned above. Furthermore, char residue of EP/SDPS/SPDM-2 composite showed greatly different morphology in contrast to above polymer systems. One can see a honeycomb structure with thick and dense carbon layer, which is the typical carbonaceous structure of intumescent flame retardancy (Fig. 10d). Such a type of architecture could greatly hamper the transfer of heat and oxygen in the combustion layer and matrix (Fig. 10d), thus leading to enhanced flame retarding performance.

In order to further reveal the microstructure of charring residue, Raman spectroscope was conducted. Fig. 11 shows the diffusion spectra of the char residues obtained from Raman spectroscopy. The samples all have two absorption bands in the Raman spectrum of G broad band (1580–1600 cm^{-1}) and D broad band (1350–1380 cm^{-1}). The D (A1g breathing mode) and G (E2g mode) peaks were assigned to disordered and oriented graphitic, respectively. As for polymers, there was no perfect graphite in the char residue which means that the char residue in condensed phase of polymers only composed of partly-graphitized or amorphous carbonaceous materials. As a result, the relative intensity ratio of the D peak to the G peak, ID/IG, reflects the degree of ordering of amorphous

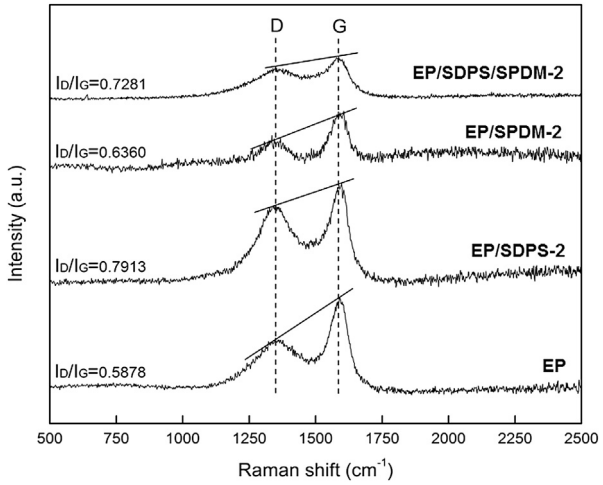

Fig. 11. Raman spectra of char residues of EP, EP/SDPS-2, EP/SPDM-2 and EP/SDPS/SPDM-2.

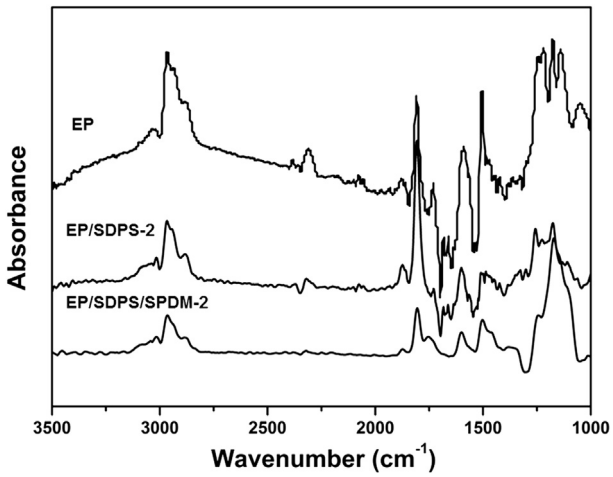

Fig. 12. TG-FTIR spectra of gas phase in the thermal degradation of Neat EP, EP/SDPS-2 and EP/SDPS/SPDM-2.

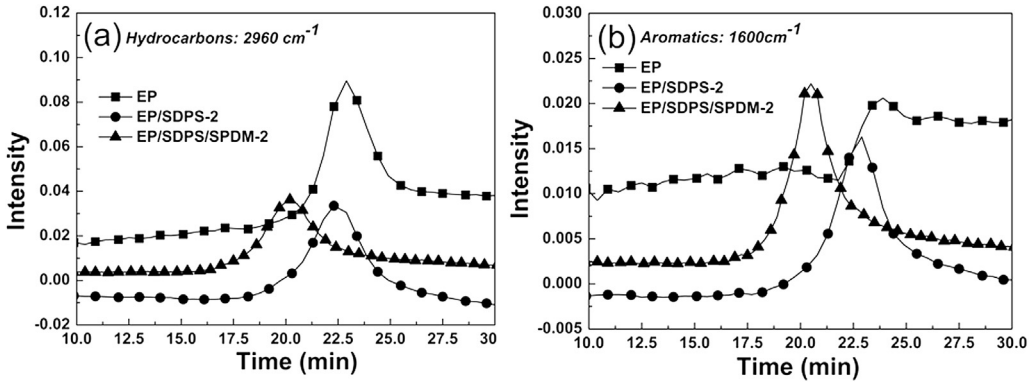

Fig. 13. The intensities of hydrocarbons and aromatics as a function of time for EP, EP/SDPS-2 and EP/SDPS/SPDM-2.

carbonaceous materials and microcrystalline planar size (La) [35]. The calculated results indicate that the charring residues of EP/SDPS/SPDM composites exhibit a larger value of ID/IG (0.73) in contrast to EP and EP/SPDM (0.59 and 0.64), implying more ordering of amorphous carbonaceous materials and larger microcrystalline planar size. This may enhance the barrier effect of carbonaceous layer.

3.8. Volatile decomposition products

TG-FTIR was used to investigate the volatilized gas during the degradation of EP and its composites. TG-FTIR spectra of gas phase in the thermal degradation of neat EP and the composites are shown in Fig. 12. The evolved gas analysis for neat EP exhibited characteristic bands of hydrocarbons (2800–3000 cm^{-1}), CO_2 (2250–2400 cm^{-1}) and aromatics (1600 and 1500 cm^{-1}), proving these to be the main decomposition products. Similar IR spectrum was found for EP/SDPS (Fig. 12), indicating an absence of a considerable change in gas evolution. In contrast, the addition of SPDM in EP/SDPS led to an obvious change in IR spectrum. The evolved gas analysis revealed that the gaseous products mainly consisted of hydrocarbons and aromatics without detection of CO_2. The absence of CO_2 in gaseous products demonstrated a great inhibition of oxidation reaction, which presented an important contribution for the enhancement in fire resistance. Moreover, the absorbance intensity of hydrocarbon and aromatics with evolution time was depicted in Fig. 13. One can find that EP/SDPS/SPDM exhibited a lower gas evolution temperature than EP and EP/SDPS. This can be easily explained by that the incorporation of SPDM facilitated the thermal degradation process as revealed in TGA and DTG. The evolution temperature of these gaseous products was in agreement with the TGA results. Furthermore, as compared with EP and EP/SDPS, one can observe a decreased intensity of hydrocarbons and an increased intensity of aromatics for EP/SDPS and EP-SDPS/SPDM-2. This result demonstrated that the cooperative use of SDPS and SPDM effectively inhibits the production of flammable gas, meanwhile, implies an enhancement in the graphitization of epoxy resin. Thus, apart from in condensed phase, the SPDS/SPDM system should also act the flame retardancy in gas phase.

4. Conclusions

A dicyclic silicon-/phosphorus-containing flame retardant was synthesized by reacting SPDPC with diphenylsilanediol (DPSD). FTIR, SEM and TGA measurements suggest that polyphosphates and silica were produced during the thermal degradation of SDPS. The cooperative use of SPDM and SDPS with the ratio of 1:1 in EP resulted in a relatively high LOI value and a relatively low PHHR. TGA analysis indicated that the enhancement in synergistic effect should be related to the high char residual weight ratio. Further, it revealed that the high char residual weight ratio is scarcely related to a facilitated char forming process. SEM images of char residue results showed a honeycomb structure with compact surface. Raman spectroscopy analysis concluded that the compactness of this protective layer may be increased with increasing the content of disordered graphite. DMA and SEM characterization of EP composites showed that the interfacial interaction between EP and SDPS/SPDM is relatively strong, which may also contribute to the improvement in char stability. TGA-FTIR analysis revealed that SDPS/SPDM also acted in gas phase by inhibiting the release of flammable gas.

Acknowledgments

This work was supported by the China-NSFC (Grant No 51107106), the Youth Foundation Incubation Program of Sichuan Province (Grant No 2011JQ0042), Postgraduate Innovation Fund Project of Southwest University of Science and Technology (Grant No 13ycjj08) and the Innovation Team Foundation Incubation Program of Sichuan Province.

Appendix A. Supplementary data

Supplementary data related to this article can be found online at http://dx.doi.org/10.1016/j.polymdegradstab.2013.12.013

References

[1] Ellis B. Chemistry and technology of epoxy resins. London: Blackie Academic and Professional; 1993.
[2] Lee H, Neville K. Handbook of epoxy resin. New York: McGraw Hill; 1967.
[3] Liu SY, Hamerton I. Recent developments in the chemistry of halogen-free flame retardant polymers. Prog Polym Sci 2002;27:1661–712.
[4] Du L, Qu B. Structural characterization and thermal oxidation properties of LLDPE/MgAl-LDH nanocomposites. J Mater Chem 2006;16:1549–54.
[5] Nishida H, Fan Y, Mori T, Oyagi N, Shirai Y, Endo T. Feedstock recycling of flame-resisting poly (lactic acid)/aluminum hydroxide composite to L, L-lactide. Ind Eng Chem Res 2005;44:1433–7.
[6] Kim J, Yoo S, Bae JY, Yun HC, Wang JH, Kong BS. Thermal stabilities and mechanical properties of epoxy molding compounds (EMC) containing encapsulated red phosphorous. Polym Degrad Stab 2003;81:207–13.
[7] Franchini E, Galy J, Gerard JF, Tabuani D, Medici A. Influence of POSS structure on the fire retardant properties of epoxy hybrid networks. Polym Degrad Stab 2009;94:1728–36.
[8] Wang X, Hu Y, Song L, Xing W, Lu H. Thermal degradation behaviors of epoxy resin/POSS hybrids and phosphorus–silicon synergism of flame retardancy. J Polym Sci Polym Phys 2010;48:693–705.
[9] Orme CJ, Klaehn JR, Harrup MK, Lash RP, Stewart FF. Characterization of 2-(2-methoxyethoxy)ethanol-substituted phosphazene polymers using pervaporation, solubility parameters, and sorption studies. J Appl Polym Sci 2005;97:939–45.

[10] Lejeune N, Dez I, Jaffres PA, Lohier JF, Madec PJ, Sopkova-de Oliveira Santos J. Synthesis, crystal structure and thermal properties of phosphorylated cyclotriphosphazenes. Eur J Inorg Chem 2008;1:138–43.
[11] Braun U, Schartel B, Fichera MA, Jäger C. Flame retardancy mechanisms of aluminium phosphinate in combination with melamine polyphosphate and zinc borate in glass-fibre reinforced polyamide 6,6. Polym Degrad Stab 2007;92(8):1528–45.
[12] Iji M, Serizawa S. Silicone derivatives as new flame retardants for aromatic thermoplastics used in electronic devices. Polym Adv Technol 1998;9:593–600.
[13] Ravadits I, Toth A, Marosi G, Marton A, Szep A. Organosilicon surface layer on polyolefins to achieve improved flame retardancy through an oxygen barrier effect. Polym Degrad Stab 2001;74(3):419–22.
[14] Wang WJ, Perng LH, Hsiue GH, Chang FC. Characterization and properties of new silicone-containing epoxy resin. Polymer 2000;41(16):6113–22.
[15] Wu CS, Liu YL, Chiu YS. Epoxy resins possessing flame retardant elements from silicon incorporated epoxy compounds cured with phosphorus or nitrogen containing curing agents. Polymer 2002;41(15):4277–84.
[16] Karrasch A, Wawrzyn E, Schartel B, Jäger C. Solid-state NMR on thermal and fire residues of bisphenol A polycarbonate/silicone acrylate rubber/bisphenol A bis(diphenyl-phosphate)/(PC/SiR/BDP) and PC/SiR/BDP/zinc borate (PC/SiR/BDP/ZnB) Part I: PC charring and the impact of BDP and ZnB. Polym Degrad Stab 2010;95:2525–33.
[17] Karrasch A, Wawrzyn E, Schartel B, Jäger C. Solid-state NMR on thermal and fire residues of bisphenol A polycarbonate/silicone acrylate rubber/bisphenol A bis(diphenyl-phosphate) (PC/SiR/BDP) and PC/SiR/BDP/zinc borate (PC/SiR/BDP/ZnB)-part II: the influence of SiR. Polym Degrad Stab 2010;95:2534–40.
[18] Wawrzyn E, Schartel B, Seefeldt H, Karrasch A, Jäger C. What reacts with what in bisphenol a polycarbonate/silicon rubber/bisphenol a bis(diphenyl phosphate) during pyrolysis and fire behavior. Ind Eng Chem Res 2012;51:1244–55.
[19] Yu D, Kleemeier M, Wu GM, Schartel B, Liu WQ, Hartwig A. Phosphorus and silicon containing low-melting organic–inorganic glasses improve flame retardancy of epoxy/clay composites. Macro Mater Eng 2011;296:952–64.
[20] Yu D, Kleemeier M, Wu GM, Schartel B, Liu WQ, Hartwig A. The absence of size-dependency in flame retarded composites containing low-melting organic–inorganic glass and clay: comparison between micro-and nanocomposites. Polym Degrad Stab 2011;96:1616–24.
[21] Chen J, Liu SM, Zhao JQ. Synthesis, application and flame retardancy mechanism of a novel flame retardant containing silicon and caged bicyclic phosphate for polyamide 6. Polym Degrad Stab 2011;96:1508–15.
[22] Sponton M, Mercado LA, Ronda JC, Galia M, Cadiz V. Preparation, thermal properties and flame retardancy of phosphorus- and silicon-containing epoxy resins. Polym Degrad Stab 2008;93:2025–31.
[23] Zhang WC, Li XM, Guo XY, Yang RJ. Mechanical and thermal properties and flame retardancy of phosphorus-containing polyhedral oligomeric silsesquioxane (DOPO-POSS)/polycarbonate composites. Polym Degrad Stab 2010;95:2541–6.
[24] Zhang WC, Li XM, Yang RJ. Novel flame retardancy effects of DOPO-POSS on epoxy resins. Polym Degrad Stab 2011;96:2167–73.
[25] Zhang WC, Li XM, Yang RJ. Blowing-out effect in epoxy composites flame retarded by DOPO-POSS and its correlation with amide curing agents. Polym Degrad Stab 2012;97:1314–24.
[26] Nizar D, Stéphane G, Eric D, Guillaume L. Development of fire resistant PET fibrous structures based on phosphinate-POSS blends. Polym Degrad Stab 2012;97:879–85.
[27] Burkhard CA. Diphenylsilanediol. In: Inorganic syntheses, vol. 3; 1950. pp. 62–3.
[28] Wang J, Li G, Yang S. New intumescent flame-retardant agent: application to polyurethane coatings. J Appl Polym Sci 2004;91:1193–206.
[29] Halpern Y. Intumescent flame retardant thermoplastic polyester compositions. US Patent 4338245; 1982.
[30] Sava BA, Elisa M, Vasiliu IC, Nastase F, Simon S. Investigations on sol-gel process and structural characterization of SiO_2-P_2O_5 powders. J Non-Crystall Sol 2012;358:2877–85.
[31] Hu XP, Guo YY, Chen L, Wang XL, Li LJ, Wang YZ. A novel polymeric intumescent flame retardant: synthesis, thermal degradation mechanism and application in ABS copolymer. Polym Degrad Stab 2012;97:1772–8.
[32] Jiang WZ, Hao JW, Han ZD. Study on the thermal degradation of mixtures of ammonium polyphosphate and a novel caged bicyclic phosphate and their flame retardant effect in polypropylene. Polym Degrad Stab 2012;97:632–7.
[33] Zhou S, Song L, Wang ZZ, Hu Y, Xing WY. Flame retardation and char formation mechanism of intumescent flame retarded polypropylene composites containing melamine phosphate and pentaerythritol phosphate. Polym Degrad Stab 2008;93(10):1799–806.
[34] Ma HY, Tong LF, Xu ZB, Fang ZP. Functionalizing carbon nanotubes by grafting on intumescent flame retardant: nanocomposite synthesis, morphology, rheology, and flammability. Adv Funct Mater 2008;18:414–21.
[35] Ferrari AC, Robertson J. Interpretation of Raman spectra of disordered and amorphous carbon. Phys Rev B 2000;61:14095–107.